CrossMark

J. Fluid Mech. (2017), *vol.* 811, *pp.* 400–420. © Cambridge University Press 2016
doi:10.1017/jfm.2016.754

Inherently unstable internal gravity waves due to resonant harmonic generation

Yong Liang[1], **Ahmad Zareei**[2] **and Mohammad-Reza Alam**[1,2,†]

[1]Applied Science and Technology, University of California, Berkeley, CA 94720, USA

[2]Department of Mechanical Engineering, University of California, Berkeley, CA 94720, USA

(Received 15 April 2016; revised 18 October 2016; accepted 7 November 2016;
first published online 13 December 2016)

Here we show that there exist internal gravity waves that are inherently unstable, that is, they cannot exist in nature for a long time. The instability mechanism is a one-way (irreversible) harmonic-generation resonance that permanently transfers the energy of an internal wave to its higher harmonics. We show that, in fact, there are a countably infinite number of such unstable waves. For the harmonic-generation resonance to take place, the nonlinear terms in the free surface boundary condition play a pivotal role, and the instability does not occur in a linearly stratified fluid if a simplified boundary condition, such as a rigid lid or a linearized boundary condition, is employed. Harmonic-generation resonance presented here provides a mechanism for the transfer of internal wave energy to the higher-frequency part of the spectrum hence affecting, potentially significantly, the evolution of the internal waves spectrum.

Key words: internal waves, nonlinear instability

1. Introduction

Internal gravity waves, an outcome of perpetually agitated density-stratified oceans, are known to play a critical role in the dynamics of our planet's energy balance: they need energy to be created, carry energy over long distances as they propagate and release energy where they break (Staquet & Sommeria 2002). The latter phenomenon usually gives rise to considerable mixing (cf. Ferrari & Wunsch 2008) whereby nutrients also get distributed, which is vital for a wide range of marine life (Boyd 2007; Harris 1986).

Research conducted for over a century has shed a lot of light on various features of internal gravity waves. Nevertheless, many aspects of their inception and fate is not yet well understood (e.g. Alford *et al.* 2015). Specifically, the precise mechanism that transfers energy from longer waves to small scales, where internal waves are more prone to breaking and being dissipated, is still a matter of dispute. Aside from linear processes such as interaction of internal waves with the seabed topography and sloped continental shelves (e.g. Zhang, King & Swinney 2008), several nonlinear instability mechanisms have also been put forward. These include, for instance, parametric subharmonic instability (e.g. Davis & Acrivos 1967; Hasselmann 1967; Scolan, Ermanyuk & Dauxois 2013), triad resonances between free propagating waves

† Email address for correspondence: reza.alam@berkeley.edu

https://doi.org/10.1017/jfm.2016.754 Published online by Cambridge University Press

(e.g. Thorpe 1968; McComas & Bretherton 1977; Jiang & Marcus 2009; Alam, Liu & Yue 2011; Wunsch 2015), and nonlinear internal wave topography interactions (e.g. Alam, Liu & Yue 2009*b*). All discovered destabilizing mechanisms for an internal wave (few named above), however, have one thing in common that they require some type of perturbations in order to get initiated. These perturbations can come from, for instance, the seabed corrugations or the presence of other waves forming resonance triads.

Here, we show that there are internal gravity waves in the ocean that are inherently unstable, that is, they simply cannot sustain their form. Through the mechanism studied here, specific internal waves naturally (without requiring any perturbation) give up their energy permanently to their higher harmonics through a one-way irreversible harmonic-generation resonance mechanism.

2. Governing equations and dispersion relation

Consider the propagation of internal waves in an inviscid, incompressible, adiabatic and stably stratified fluid of density $\rho(x, y, z, t)$, bounded by a free surface on the top and a rigid sea floor at the depth h. Let's define a Cartesian coordinate system with x, y-axes on the mean free surface and z-axis positive upward. Newton's second law, conservation of mass and conservation of salt provide five equations for the evolution of the components of the velocity vector $\boldsymbol{u} = \{u, v, w\}$, density ρ and the pressure p. These governing equations under Boussinesq approximation together with three boundary conditions (two kinematic boundary conditions on the free surface and the seabed, and one dynamic boundary condition on the free surface) uniquely determine the five unknowns and the surface elevation $\eta(x, y, t)$ (e.g. Thorpe 1966).

We assume internal waves are small perturbations to a stable background state at equilibrium. Therefore, density can be written as $\rho(x, y, z, t) = \bar{\rho}(z) + \rho'(x, y, z, t)$ where $\bar{\rho}(z)$ is the background (unperturbed) density. Similarly, we define a pressure perturbation p' via $p = \bar{p}(z) + p'(x, y, z, t)$ such that $\mathrm{d}\bar{p}(z)/\mathrm{d}z = -\bar{\rho}(z)g$. With some standard manipulation, the governing equations can be written in terms of any of the five variables involved in this problem. We choose to write the equation, as is customary, in terms of the vertical component of the velocity, w. These equations then read (see e.g. Thorpe 1966, or appendix A)

$$\frac{\partial^2}{\partial t^2}\nabla^2 w + N^2\nabla_H^2 w = \mathcal{E}(\boldsymbol{u}, \rho'), \quad -h < z < \eta, \tag{2.1a}$$

$$\frac{\partial^3 w}{\partial z \partial t^2} - g\nabla_H^2 w = \mathcal{F}(\boldsymbol{u}, p', \eta), \quad z = 0, \tag{2.1b}$$

$$w = 0, \quad z = -h, \tag{2.1c}$$

where $\nabla_H^2 = \partial^2/\partial x^2 + \partial^2/\partial y^2$ is the horizontal Laplacian, $N^2 = -(g/\rho_0)\,\mathrm{d}\bar{\rho}(z)/\mathrm{d}z$ is the Brunt–Väisälä frequency in which $\rho_0 = \bar{\rho}(z = 0)$ is the density on the free surface and $\mathcal{E}, \mathcal{F}$ are nonlinear functions of their arguments.

To perform a perturbation analysis, we assume that the solution to (2.1) can be expressed in terms of a convergent series, i.e.

$$w(\boldsymbol{x}, t) = \epsilon w^{(1)}(\boldsymbol{x}, t) + \epsilon^2 w^{(2)}(\boldsymbol{x}, t) + O(\epsilon^3), \tag{2.2}$$

where $\epsilon \ll 1$ is a measure of steepness of the waves involved and $w^{(i)} \sim O(1)$. Similar expressions hold for u, v, ρ' and p'. Substituting (2.2) into (2.1) and collecting terms of the same magnitude, then at the leading order $O(\epsilon)$ the linearized equations are obtained.

https://doi.org/10.1017/jfm.2016.754 Published online by Cambridge University Press

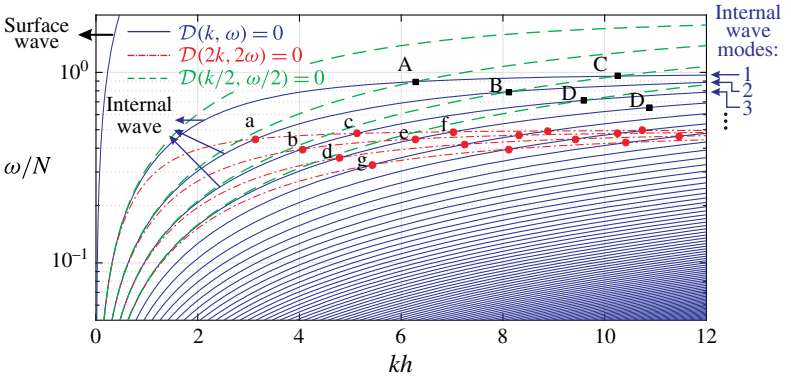


FIGURE 1. (Colour online) Plot of the dimensionless frequency ω/N as a function of dimensionless wavenumber kh of free internal waves (i.e. $\mathcal{D}(k,\omega)=0$) in a fluid of linearly stratified density $\rho(z)=\rho_0(1-az)$, with $ah=0.05$. Associated with each wavenumber there is one surface wave and an infinite number of internal wave modes (blue solid-line branches). The frequency of internal waves cannot exceed the Brunt–Väisälä frequency N, and all branches of the dispersion relation curve are capped at $\omega/N=1$. We also plot contours of $\mathcal{D}(2k,2\omega)=0$ (red dash-dotted lines) whose intersections with blue lines (shown by red circles) mark waves whose second harmonics are also solutions to the dispersion relation. These second harmonics are at the intersections of contours of $\mathcal{D}(k/2,\omega/2)=0$ (green dashed lines) and $\mathcal{D}(k,\omega)=0$ and are marked by black squares. The second harmonic of the wave at 'a' (mode 2), is the wave 'A' (mode 1) and so on.

We focus our attention here on the two-dimensional problem with a linear mean density profile, i.e. $\bar{\rho}(z)=\rho_0(1-az)$ which gives a constant Brunt–Väisälä frequency $N=\sqrt{ga}$ (cf. e.g. Martin, Simmons & Wunsch 1972). Looking for a progressive wave solution of the leading-order (linearized) equation in the form $w^{(1)}=W(z)\sin(\boldsymbol{k}\cdot\boldsymbol{x}-\omega t)$ the following dispersion relations result:

$$\mathcal{D}(k,\omega)=\begin{cases}\omega^2-\dfrac{gk}{\sqrt{1-N^2/\omega^2}}\tanh\left(kh\sqrt{1-N^2/\omega^2}\right)=0, & \omega>N\\ \omega^2-\dfrac{gk}{\sqrt{N^2/\omega^2-1}}\tan\left(kh\sqrt{N^2/\omega^2-1}\right)=0, & \omega<N.\end{cases}\tag{2.3}$$

Solutions to the above dispersion relation identify permissible frequencies and wavenumbers of free propagating waves. Contours of $\mathcal{D}(k,\omega)=0$ are shown in figure 1 in which we plot the dimensionless frequency ω/N as a function of dimensionless wavenumber kh (blue solid curves). For $\omega>N$ only one solution exists in the first quadrant (with its mirror in the other quadrants). This solution corresponds to a wave whose associated fluid particle motion is maximum near the free surface and decreases as the depth increases. Therefore this is basically a classical surface wave which is perturbed slightly because of stratification. For $\omega<N$ there is an infinite number of solutions to (2.3). The first member of this set, is the continuation of the surface wave branch (the leftmost branch in figure 1), but the rest identify waves with associated fluid particles' vertical velocities w that are zero at the seabed and close to zero near the free surface, but gain one (or more) maximum/maxima somewhere inside the fluid domain. Therefore these branches show

https://doi.org/10.1017/jfm.2016.754 Published online by Cambridge University Press

internal waves. The number of maxima in the amplitude of the vertical velocity w along the vertical water line determines the mode number of the branch (the first three are marked on the right-hand side of figure 1 with arrows). A cutoff frequency $\omega/N = 1$ sets an upper frequency limit for internal waves. We would like to emphasize that the free surface boundary condition, in comparison with the rigid-lid case, leads to a drastically different expressions for mode structures and the dispersion relation. Nevertheless, the curves of the dispersion relation (2.2) are very close to the one under the rigid-lid assumption $\omega = N/\sqrt{1 + (n\pi/kh)^2}$.

It can be seen from figure 1 that second-harmonic waves are at least one mode lower than the original waves. Therefore, clearly a mode-1 internal wave can never generate a second harmonic, since its second harmonic must be a mode zero which is non-existent. But mode-2 internal waves can go unstable and resonate mode-1 waves. Therefore, in an internal wave spectrum, there might be mode-1 waves whose origin is different from the origin of the rest of the incident mode-1 internal waves; that is, they are results of instability of mode-2 (and other higher modes) internal waves.

We would like to comment that the dominant energy in the baroclinic tide, which is the most relevant case for the ocean, is in the mode-1 waves. However, most of the prevalent low-mode internal waves (including mode 1) are eventually dissipated through their energy being transferred to waves with higher vertical wavenumbers (see e.g. Garrett 2003). This happens through a number of mechanisms including, for instance, parametric subharmonic instability (aka PSI, e.g. Davis & Acrivos 1967) and interaction with the bottom topography (e.g. Bühler & Holmes-Cerfon 2011; Couston, Liang & Alam 2016; Karimpour, Zareei & Alam 2016). Resonant harmonic generation studied here may interfere, potentially substantially, in this process of energy exchange between different modes. In other words, the mechanism studied here can influence the internal wave spectral evolution by opening up a new avenue for the energy exchange between different modes.

3. Harmonic generation

With the linear solution to (2.1) and its properties at hand, we move to the second-order equation by collecting $O(\epsilon^2)$ terms obtained from the substitution of (2.2) into (2.1). The second-order equation has the exact same form as of the leading-order equation on its left-hand side, but with nonlinear terms, arising from the nonlinear functions $\mathcal{E}$, $\mathcal{F}$, on its right-hand side. These nonlinear terms are multiplication of the linear solution (and its derivatives) and, it turns out that, they constitute forcing terms with wavenumber and frequency $(2k, 2\omega)$. Now if $\mathcal{D}(2k, 2\omega) = 0$, then it means that these forcing terms have a harmonic which is the same as the natural harmonic of the linear system. This is a resonance scenario through which a new second-order solution may emerge and may grow large enough to the extent that it becomes comparable to the leading-order solution. We would like to note a subtle point here that at the second order the right-hand side of (2.1*a*) is identically zero (see e.g. Tabaei, Akylas & Lamb 2005). Therefore a potential harmonic-generation resonance is only possible through the nonlinear terms in the free surface boundary condition (2.1*b*). If a rigid-lid assumption or a linearized form of the free surface boundary condition is employed (which is usually the case in the investigation of internal waves) the resonance harmonic generation will simply not obtain unless a non-uniform stratification or Boussinesq terms are considered.

To see whether it is possible to satisfy the resonance condition required for the second harmonic of an internal wave to exist as a free propagating wave, we also

https://doi.org/10.1017/jfm.2016.754 Published online by Cambridge University Press

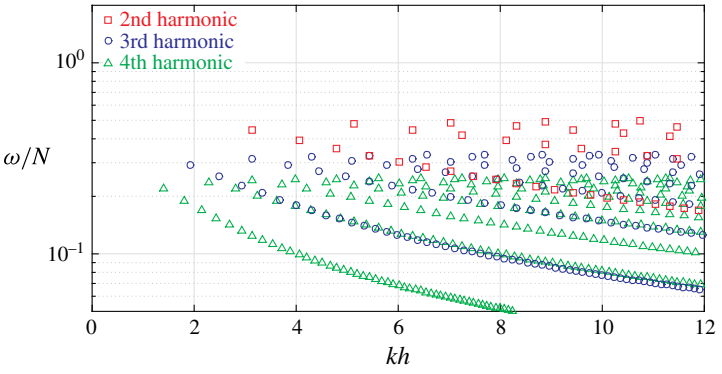


FIGURE 2. (Colour online) There are countably infinite number of internal waves that are unstable to their second harmonic. Physically this means that specific incident internal waves of wavenumber and frequency (k, ω) will give up their energy permanently (in a one-way irreversible process, cf. (4.2)) to their second harmonic $(2k, 2\omega)$. The necessary condition for this to happen is $\mathcal{D}(k, \omega) = \mathcal{D}(2k, 2\omega) = 0$. These waves, for the parameters of figure 1, are shown here by red squares. Similar story holds for another set of waves that are unstable to their third harmonic (blue circles, necessary condition $\mathcal{D}(k, \omega) = \mathcal{D}(3k, 3\omega) = 0$) and fourth harmonic (green triangles, $\mathcal{D}(k, \omega) = \mathcal{D}(4k, 4\omega) = 0$) and so on.

plot in figure 1 the contours of $\mathcal{D}(2k, 2\omega) = 0$ (red dash-dotted curves) for the first four internal wave modes. Intersections of these contours with the contours of $\mathcal{D}(k, \omega) = 0$ (solid blue curves) identify waves whose second harmonics are also solutions to the dispersion relation. Some of these intersections are marked in figure 1 by red circles and are identified by lowercase characters. It is easy to find the corresponding second harmonic by multiplying a designated (red circle) frequency and wavenumber by a factor of two, or alternatively by finding intersections of contours of $\mathcal{D}(k/2, \omega/2) = 0$ (green dashed curves) and $\mathcal{D}(k, \omega)$ (denoted by black squares and uppercase characters). Specifically, 'A' is the second harmonic of 'a', 'B' is the second harmonic of 'b' and so on. It is to be noted that the second harmonic of an internal wave always belongs to a lower mode than the mode of the original wave. For example, the second harmonic of wave 'a' (mode 2) is the wave 'A' (mode 1) and the second harmonic of wave 'c' (mode 3) is the wave 'C' (mode 1).

A comprehensive collection of all internal waves (for $kh < 12$) whose second harmonics are also free propagating waves is shown in figure 2. We are basically plotting in this figure all intersections points of contours of $\mathcal{D}(k, \omega) = 0$ and contours of $\mathcal{D}(2k, 2\omega) = 0$. Clearly there will be an infinite (but countable) number of such solutions. Through the approach described above, a similar exercise can be performed for waves with their third harmonic being free waves. These solutions are marked by blue circles in figure 2, and waves with their fourth harmonics lying on the dispersion relation curves are shown by green triangles, and this search can continue indefinitely. In a weakly nonlinear wave propagation problem, instabilities to higher harmonics (e.g. third, fourth, etc.) are much weaker compared with the instability to the second harmonic. This is because the expression for the amplitude growth of higher harmonics contains higher-order perturbation terms. Specifically, if ϵ is a measure of a wave steepness, then the amplitude growth rate of its second-harmonic wave is of $O(\epsilon^2)$, but if its third harmonic is excited, then the growth rate is of $O(\epsilon^3)$ (cf. the difference between Class I and Class II/III Bragg resonance, e.g. Alam, Liu & Yue 2009*a*).

https://doi.org/10.1017/jfm.2016.754 Published online by Cambridge University Press

4. Results and discussion

To determine the strength of the resonance (i.e. the rate of growth of the resonant wave), and the dynamics of the energy interplay between a wave and its second harmonic, here we perform a multiple scale perturbation analysis. The basic assumption is that the original wave and its second harmonic are both functions of spatial variables and time (i.e. $\boldsymbol{x}$, t), as well as a slow spatial variable in the direction of propagation $x_1 = \epsilon x$. Physically speaking, we allow the amplitude of both waves to slowly vary as waves propagate. Mathematically speaking this is written as

$$w(x, x_1, z, t) = \epsilon w_1(x, x_1, z, t) + \epsilon^2 w_2(x, x_1, z, t) + O(\epsilon^3), \tag{4.1}$$

where $w_i \sim O(1)$. Expressions of the same form are assumed to hold for other variables u, ρ', p' and η. Similar to regular perturbation methodology, described earlier in the paper to gain insight into the problem, we substitute (4.1) into the governing equation (2.1) and collect terms of the same order in ϵ. We assume the original wave with wavenumber and frequency k, ω has the amplitude $\mathcal{A}_1(x_1)$ and the amplitude of resonant second-harmonic wave with wavenumber and frequency $2k$, 2ω is $\mathcal{B}_2(x_1)$. At the second order, applying a compatibility condition (to avoid unbounded solutions) the following two equations governing spatial evolution of $\mathcal{A}_1(x_1)$ and $\mathcal{B}_2(x_1)$ emerge (see appendix A for details of derivation)

$$\frac{\mathrm{d}\mathcal{B}_2(x_1)}{\mathrm{d}x} = \alpha \mathcal{A}_1^2(x_1), \tag{4.2a}$$

$$\frac{\mathrm{d}\mathcal{A}_1(x_1)}{\mathrm{d}x} = \beta \mathcal{A}_1(x_1)\mathcal{B}_2(x_1), \tag{4.2b}$$

where

$$\alpha = -\frac{6m_1^2\omega \cos m_2 h}{gk(2m_2 h + \sin 2m_2 h)}, \tag{4.3}$$

$$\beta = -\frac{k[\sin m_2 h(4m_1 \cos^2 m_1 h - 3m_1) - 2m_2 \cos m_2 h \sin 2m_1 h]}{2\omega(2m_1 h + \sin 2m_1 h)}, \tag{4.4}$$

in which $m_1 = k\sqrt{N^2 - \omega^2}/\omega$ and $m_2 = k\sqrt{N^2 - 4\omega^2}/\omega$.

Spatial evolution of the normalized amplitude of the original wave $\mathcal{A}_1/\mathcal{A}_{10}$ (where $\mathcal{A}_{10} = \mathcal{A}_1(x = 0)$) and its second harmonic $\mathcal{B}_2/\mathcal{A}_{10}$ as a function of spatial distance of propagation x/λ_i (where $\lambda_i = 2\pi/k =$ wavelength of the original wave) is shown in figure 3 respectively by blue-dashed line and solid-red line. In accordance with the case presented in figure 1, we choose $ah = 0.05$ and we consider that waves are propagating in a water of depth $h = 1$ km, then $N = 0.02$ rad s^{-1}. For this case, figure 3(*a*) corresponds to the point 'a' ($kh = 3.144772$, $\omega/N = 0.4472136$) with its second harmonic at 'A' in figure 1, and figure 3(*b*) corresponds to point 'c' ($kh = 5.132426$, $\omega/N = 0.4780914$) with its second harmonic at 'C'. In the former case the interaction is (spatially) faster by a factor of approximately two, while in the latter case, the relative amplitude of the resonant wave is higher. The most striking aspect of the solution is that the interaction is one way. This can be seen from (4.2*a*) in which, because $\mathcal{A}_1^2$ is always positive, then $\mathrm{d}\mathcal{B}_2/\mathrm{d}x_1$ can never change sign. As a result the magnitude of $\mathcal{B}_2$ can only increase (the sign of α only contributes to 0 or π radian phase shift to the wave), and that is why the direction of energy can never change.

https://doi.org/10.1017/jfm.2016.754 Published online by Cambridge University Press

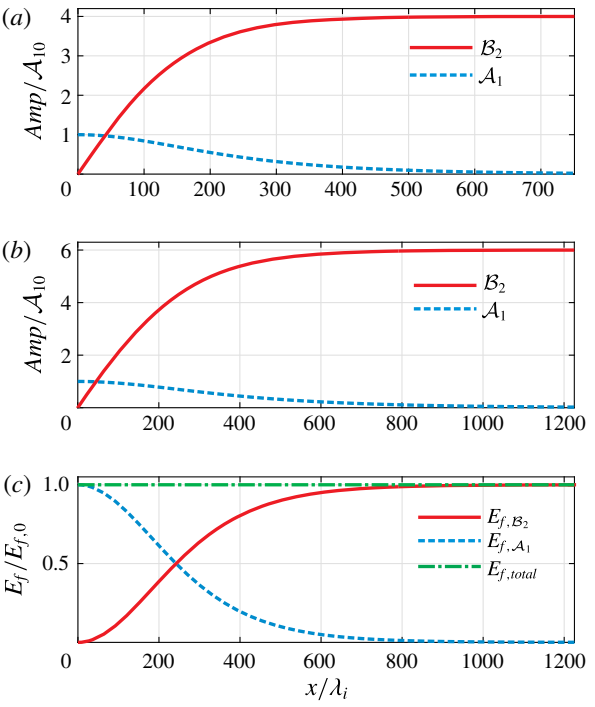


FIGURE 3. (Colour online) Spatial evolution of the amplitude of the original wave (blue dashed line) and its resonant second harmonic (red solid line) corresponding to the point 'a' in figure 1 ($kh = 3.144772$, $\omega/N = 0.4472136$, $aA_{10}/N = 0.0023$, a) and the point 'c' in figure 1 ($kh = 5.132426$, $\omega/N = 0.4780914$, $aA_{10}/N = 0.0023$, b). In (a) energy goes from mode 2 to mode 1, whereas in (b) energy goes from mode 3 to mode 1. (c) The energy flux of each wave as well as the sum of the energy fluxes (green dash-dotted line) in case (b). As expected from energy conservation, the overall energy flux is unchanged in the domain of interaction.

This is in contrast to typical triad resonance interactions (e.g. McComas & Bretherton 1977; Alam, Liu & Yue 2010; Alam 2012) and harmonic generation in shallow water waves (e.g. Alam & Mei 2007) where energy initially flows from original waves to resonant waves, but then when the amplitude of resonant waves is large enough the flow of energy reverses. Here, energy only goes from the original wave to the second harmonic and stays there permanently. The original wave will be gone forever.

Our multiple scales results conserve energy, as expected. In figure 3(c) (which corresponds to the case presented in figure 3b) we plot the energy flux ($E_f = E \times C_g$ where E is the energy per unit horizontal area and C_g is the group velocity) normalized by the energy flux of the original wave at the beginning ($E_{f,\mathcal{A}_{10}}$). Plotted are the normalized energy flux of the original wave $E_{f,\mathcal{A}_1}$ (blue-dashed line), the second harmonic $E_{f,\mathcal{B}_2}$, and the summation of the fluxes $E_{f,total} = E_{f,\mathcal{A}_1} + E_{f,\mathcal{B}_2}$. As expected from the conservation of energy the latter is constant and equal to unity.

To cross-validate our results with direct simulation, we use the adaptive Navier–Stokes solver code SUNTANS (Stanford Unstructured Nonhydrostatic Terrain-following Adaptive Navier–Stokes Simulator (Fringer, Gerritsen & Street 2006)). As a non-hydrostatic parallel ocean model with the capability to implement a nonlinear free surface, SUNTANS has been validated and widely used in studying

https://doi.org/10.1017/jfm.2016.754 Published online by Cambridge University Press

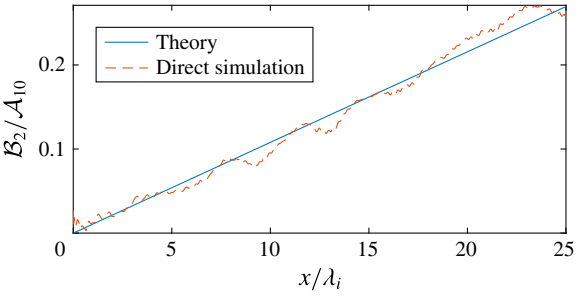


FIGURE 4. (Colour online) Comparison of analytical results (4.2) with the direct simulation. The physical parameters used are: density gradient $a = 1 \times 10^{-3}$ m^{-1}, water depth $h = 100$ m, dimensionless wavenumber $kh = 3.147946$, dimensionless frequency $\omega/N = 0.4472136$, the amplitude of vertical velocity of the incident wave $A_{10} = 0.1$ m s^{-1}.

internal waves (and associated turbulence and mixing) in stratified waters (Kang & Fringer 2010; Wang *et al.* 2011; Zhang, Fringer & Ramp 2011; Kang & Fringer 2012; Walter *et al.* 2012).

Here we consider propagation of waves in a stratified water of density gradient $a = 1 \times 10^{-3}$ m^{-1} (i.e. $N = 0.1$ rad s^{-1}), depth 100 m and in a domain of horizontal extent 20 km. We choose 5×10^3 grid points in the x direction and 100 layers in the z direction. We specify the velocity of fluid particles at the left boundary to match that of desired incoming wave. Therefore the left boundary that serves as the incoming wave boundary (wave maker). The right boundary is closed and a slip-free boundary condition is applied. We consider the case of an incident internal wave of mode 2 ($kh = 3.147946$, $\omega/N = 0.4472136$ vertical velocity amplitude $w = 0.1$ m s^{-1}) with its second harmonic being a mode-1 wave. The time step $\delta t/T = 1/35000$ where T is the period of the incident wave. We run the simulation until the incident wave arrives at the wall, at which point the amplitude of both waves (incident and its second harmonics) have reached a steady state in the domain of interest $0 < x/\lambda_i < 20$. As is seen from figure 4, the curve of $\mathcal{B}_2/\mathcal{A}_{10}$ vs x/λ_1 gives an initial slope of 0.0107 which is the same as our theoretical prediction (4.2).

To see how fast this instability evolves temporally, we present in figure 5 results of the temporal evolution of the parent wave and its second harmonic, with the same physical parameters as in the case in figure 3(*a*). The governing equation takes a similar form to (4.2) except the derivatives that are with respect to the time t and clearly expressions for α and β are different. The qualitative trend is as the spatial case, and the figure suggests that we need time $\sim O(1000)$ times the period of the initial wave to see the majority of the energy transmitted to the second harmonic. With the chosen Brunt–Väisälä frequency of $N = 0.022$ s^{-1} (correspondingly, the wavenumber is $k = 3.14 \times 10^{-3}$ m^{-1}, the frequency is 9.90×10^{-3} s^{-1}, the wave amplitude is 1 m, the water depth is 1000 m and $a = 5 \times 10^{-5}$ m^{-1}), the time scale is approximately 10 days, which is of the same order as that of parametric subharmonic instability of the M2 internal tide (~2–5 days) (cf. e.g. MacKinnon & Winters 2005; Gerkema, Staquet & Bouruet-Aubertot 2006). This is somewhat expected as both mechanisms are second-order resonance instabilities. Similar to the spatial case, the governing equation is,

$$\frac{\mathrm{d}\mathcal{B}_2(t_1)}{\mathrm{d}t} = \alpha_t \mathcal{A}_1^2(t_1), \tag{4.5a}$$

https://doi.org/10.1017/jfm.2016.754 Published online by Cambridge University Press

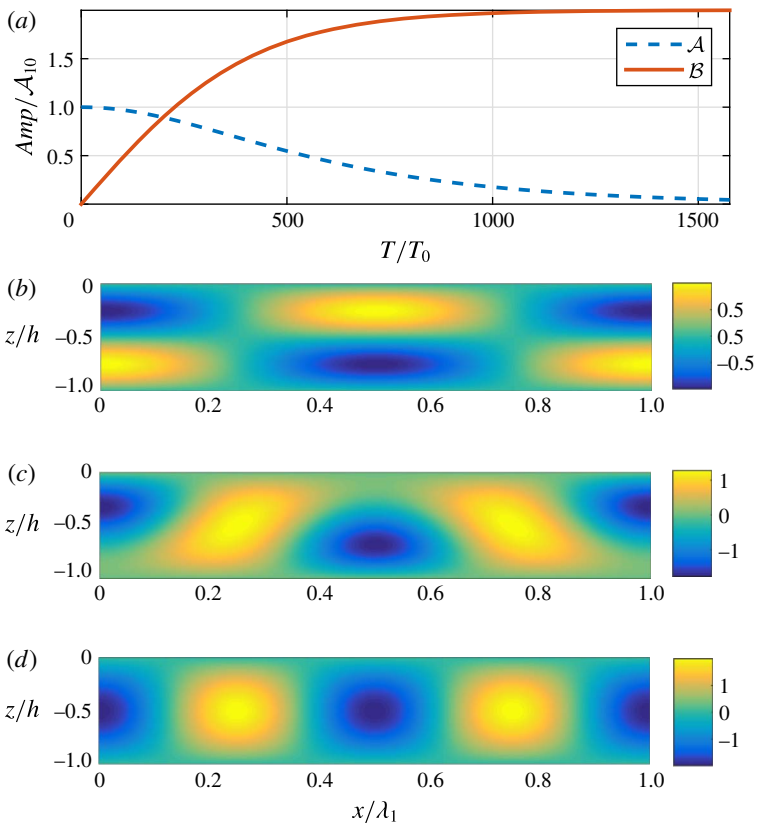


FIGURE 5. (Colour online) Time evolution of the vertical velocities of internal gravity waves that satisfy the conditions of harmonic generation. The physical parameters used here correspond to figure 3(*a*). (*a*) Time evolution of the amplitudes of the two waves. T_0 is the period of the parent wave. (*b–d*) Snapshots of the wave field at $t = 0$ (*b*), $t = 500T_0$ (*c*) and $1500T_0$ (*d*). The presented mechanism initially results in a modulation of the primary wave, and eventually all the energy goes to the second harmonic.

$$\frac{\mathrm{d}\mathcal{A}_1(t_1)}{\mathrm{d}t} = \beta_t \mathcal{A}_1(t_1)\mathcal{B}_2(t_1), \tag{4.5b}$$

where,

$$\alpha_t = -\frac{3\omega^2 m_1^2 m_2^2 \cos m_2 h}{gk^2[m_2^3 h + 4m_2 hk^2 + (m_2^2 - 4k^2)\sin m_2 h \cos m_2 h]}, \tag{4.6}$$

$$\beta_t = -\frac{m_1 \sin m_2 h[(3m_1^2 + m_2^2 + 3k^2)\cos^2 m_1 h - 2m_1 m_2 \cot m_2 h \sin 2m_1 h - (2m_1^2 + m_2^2 + 3k^2)]}{2[2m_1^3 h + 2m_1 hk^2 + (m_1^2 - k^2)\sin 2m_1 h]}. \tag{4.7}$$

The analytical solutions to (4.5) read,

$$\mathcal{A}_1 = A_{10}\mathrm{sech}(A_{10}\sqrt{-\alpha_t\beta_t}t), \tag{4.8a}$$

$$\mathcal{B}_2 = -\frac{A_{10}\sqrt{-\alpha_t\beta_t}\tanh(A_{10}\sqrt{-\alpha_t\beta_t}t)}{\beta_t}, \tag{4.8b}$$

https://doi.org/10.1017/jfm.2016.754 Published online by Cambridge University Press

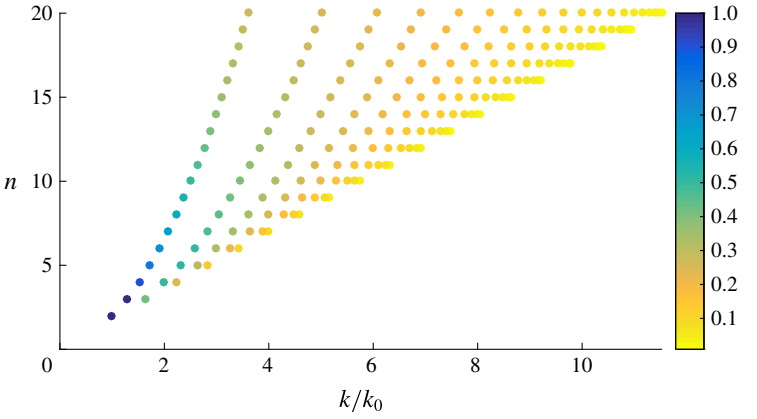


FIGURE 6. (Colour online) Dependence of the decay rate $R=\sqrt{-\alpha_t\beta_t}$ on mode numbers n and the horizontal wavenumbers. We normalize the quantities by the wave where the largest decay rate is obtained (here it corresponds to point 'a' in figure 1). Colour scale represents R/R_0 where $R_0=3.81\times10^{-6}$ m^{-1}. The physical parameters used here are the same as in figure 1.

where $A_{10}=\mathcal{A}_1(t=0)$. For instance, the time it takes for $\mathcal{A}_1$ to lose 95 % of the original amplitude is $3.69/(A_{10}\sqrt{-\alpha_t\beta_t})$ seconds. That is, the time scale for $\mathcal{A}_1$ to decay is inversely proportional to the initial wave amplitude. Given an initial wave amplitude, in figure 6 we plot the dependence of the decay rate $R=\sqrt{-\alpha_t\beta_t}$ (although physically $A_{10}\sqrt{-\alpha_t\beta_t}$ represents the actual decay rate) on mode numbers n and the horizontal wavenumbers. It can be seen that starting from the reference point (where the largest decay rate is obtained) the decay rate decreases as mode number and horizontal wavenumbers increase.

We would like to comment here that parametric subharmonic instability (PSI) is dependent upon perturbation waves in the domain in order to get started (Davis & Acrivos 1967; Muller 1986). For a monochromatic standing wave that is not an exact solution to the fully nonlinear governing equation, for PSI to occur, perturbations are still required since otherwise no subharmonic waves would be excited (see e.g. p. 436 McEwan 1971). In direct simulations, this is achieved by adding random noise to the simulation domain. In experimental studies the required noise already exists in the domain due to unavoidable imperfections. Hence, usually in experiments PSI is automatically obtained (similar to inevitable Benjamin–Feir instability) and destabilizes 'single' internal waves to a number of other subharmonic waves (e.g. Martin *et al.* 1972). We would like to emphasize that the underlying mechanism of resonant harmonic generation studied here is different than that of PSI in that the former mechanism, among other characteristics, is an 'inherent' instability that does not require ambient perturbations to get started.

Three snapshots of the overall vertical velocity w are shown in figure 5(*b–d*) that highlights the horizontal and vertical structures of the wave field at different times. Energy goes from the original internal wave (*b*) slowly to its higher harmonics, first leading to modulation of the original wave (*c*), but eventually the entire energy is at the second harmonic (*d*) whose frequency and horizontal wavenumber are double the horizontal frequency and wavenumber of the initial wave. The interaction is only

https://doi.org/10.1017/jfm.2016.754 Published online by Cambridge University Press

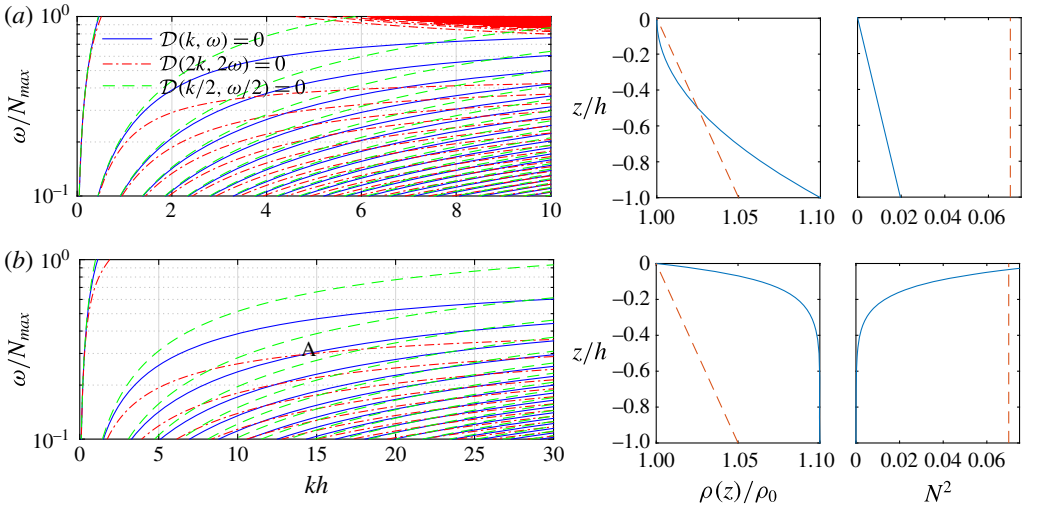


FIGURE 7. (Colour online) Plots of $\mathcal{D}(k,\omega)=0$, $\mathcal{D}(2k,2\omega)=0$ and $\mathcal{D}(k/2,\omega/2)=0$ for parabolic and exponential density profiles (cf. figure 1): (*a*) for $\rho(z)=\rho_0(1+az^2)$ with $a=1\times10^{-5}$ m^{-2} and (*b*) for $\rho(z)=\rho_0[1+\delta-\delta\exp(az)]$ with $a=0.1$ m^{-1} and $\delta=0.1$. On the right-side of each plot, we show the normalized density profile $\rho(z)/\rho_0$ and the Brunt–Väisälä frequency $N(z)^2$ of the two nonlinear density profiles (blue solid lines) overlaid of top of corresponding plots of linear density profile (red dashed lines). Water depth is $h=100$ m.

between the initial wave and its second harmonic, and no cascading to different waves ensues.

We would like to note that the harmonic-generation mechanism proposed here occurs for non-uniformly stratified ocean as well. As pointed out previously, a necessary condition for this to occur is that for a given wave of frequency ω and wavenumber k, the two conditions $\mathcal{D}(k,\omega)=0$ and $\mathcal{D}(2k,2\omega)=0$ are satisfied. We present two examples in figure 7 for two different density profiles: parabolic $\rho(z)=\rho_0(1+az^2)$, where $a=1\times10^{-5}$ m^{-2} (figure 7*a*) and exponential $\rho(z)=\rho_0[1+\delta-\delta\exp(az)]$, where $a=0.1$ m^{-1}, $\delta=0.1$ (figure 7*b*). The water depth is 100 m for both. The Brunt–Väisälä frequencies increase with depth in one case and decrease in the other. It can been seen from figure 7 that there are, as well, infinitely countable intersections (i.e. solutions) between the two sets of curves. In these cases, contrary to the constant N case, the linear wave solution does not satisfy the nonlinear Boussinesq–Euler equation and hence inclusion of the nonlinear free surface condition is not necessary for the harmonic generation to appear. The analysis for these two cases can be carried out by following the same logic presented in appendix A, although mathematically more involved and closed-form explicit solutions will be tedious, if not impossible, to obtain.

As discussed above, when density profile is not uniform and hence N is not constant, two sources contribute to the harmonic generation: (i) nonlinearities in the free surface boundary condition, i.e. right-hand side of equation (A 8*b*) and (ii) nonlinear terms in the momentum equation, i.e. right-hand side of equation (A 8*a*). As presented before, for a constant N case the latter source is absent. For non-uniform stratifications, it is of interest to evaluate the relative importance of these

https://doi.org/10.1017/jfm.2016.754 Published online by Cambridge University Press

two contributors. The motivation is to see whether the classical rigid-lid assumption would be a good approximation in estimating energy exchange due to harmonic generation when the density profile is non-uniform.

We comment on this question briefly by considering the exponential density profile as it is representative of actual pycnoclines. For such a density profile, the vertical structure of an internal wave $W(z)$ is obtained as

$$W(z) = -\frac{J_\nu(\mu)Y_\nu(p) - Y_\nu(\mu)J_\nu(p)}{Y_\nu(\mu)}, \tag{4.9}$$

where, J and Y are Bessel function of the first and the second kind respectively, and

$$\nu = \frac{2k}{a}, \quad \mu = \frac{2k\sqrt{g\delta}\mathrm{e}^{-1/2ah}}{\omega\sqrt{a}}, \quad p = \frac{2k\sqrt{g\delta}\mathrm{e}^{1/2az}}{\omega\sqrt{a}}. \tag{4.10a–c}$$

By substituting this equation into the right-hand side of equations (A 8*a*) and (A 8*b*) the relative importance of the right-hand side of the two equations are obtained.

We consider a wave with the wavenumber and frequency $kh = 14.14$ and $\omega/N_{max} = 0.30$ corresponding to the point highlighted by the character 'A' in figure 7(*b*). Averaged over the z direction, the relative magnitude of nonlinear terms on the right-hand side of the Boussinesq–Euler equation to those of free surface boundary condition (i.e. (A 8*a*) to (A 8*b*)) is only approximately 5 %. This stresses that even in the case of a nonlinear density stratification, the amplitude of nonlinear free surface terms is still much higher (here more than an order of magnitude) than those arising from the nonlinearity of the density profile. It is to be noted that in the nonlinear cases studied in figure 7, Brunt–Väisälä frequencies are significantly different from the linear case. Specifically, in both nonlinear cases, N reaches zero whereas in the linear case N is constant. Clearly the effect of a nonlinear density profile is increased as the profile departs further from a linear one.

We also would like to emphasize that the resonant harmonic generation studied here is different from non-resonant harmonic generation that occurs in non-uniform stratifications (e.g. Sutherland 2016). The former occurs for specific internal waves, transfers the entire energy to the second harmonic and is a one-way process, whereas the latter obtains for all internal waves but since it is non-resonant only transfers a portion of energy from the initial wave to the superharmonics.

We also would like to note that non-Boussinesq effects (and corresponding terms in the governing equation) can also lead to the generation of resonant super harmonics. In other words, harmonic generation can be obtained in uniform stratification with the rigid lid, if non-Boussinesq terms are not neglected. However, as will be shown shortly, the relative importance of such routing of energy is orders of magnitude less than that of nonlinear free surface avenue: following the same procedure for getting (A 2), except not making Boussinesq approximation, we obtain,

$$\begin{aligned}
&\rho\frac{\partial}{\partial t}\nabla^2 w + \rho\nabla_H^2(\boldsymbol{u}\cdot\nabla w) - \rho\frac{\partial^2}{\partial x\partial z}(\boldsymbol{u}\cdot\nabla u) - \rho\frac{\partial^2}{\partial y\partial z}(\boldsymbol{u}\cdot\nabla v) + g\nabla_H^2\rho \\
&\quad + 2\nabla\rho\cdot\nabla\frac{\partial w}{\partial t} + \frac{\partial w}{\partial t}\nabla^2\rho + 2\nabla\rho\cdot\nabla(\boldsymbol{u}\cdot\nabla w) + \nabla^2\rho\cdot(\boldsymbol{u}\cdot\nabla w) - \frac{\partial}{\partial z}\left(\frac{\partial\boldsymbol{u}}{\partial t}\cdot\nabla\rho\right) \\
&\quad - \frac{\partial}{\partial z}[\nabla\rho\cdot(\boldsymbol{u}\cdot\nabla\boldsymbol{u})] - \frac{\partial}{\partial z}\left(\frac{\partial\boldsymbol{u}}{\partial t}\cdot\nabla\rho\right) = 0.
\end{aligned} \tag{4.11}$$

https://doi.org/10.1017/jfm.2016.754 Published online by Cambridge University Press

Comparing the Boussinesq terms in the above equation and the quadratic terms on the free surface boundary condition, i.e. (A 7), we find that their ratio is of the order of a/k. For the two cases presented above, the ratios are less than 1.6 %.

The harmonic generation through a nonlinear free surface involves two energy transfer processes simultaneously, in one process (k, ω) wave loses energy to $(2k, 2\omega)$ wave and generates the second harmonic; in the other the $(2k, 2\omega)$ wave forms a triad resonance with (k, ω) wave and sends energy back in an opposite way. The triad resonance condition is clearly satisfied since $2\omega - \omega = \omega$ and $2k - k = k$. If at the initial moment we only have (k, ω) wave (i.e. no second harmonic in the domain) then harmonic generation triumphs over triad resonance in transferring energy, resulting in the combined effect that energy only goes in one direction. But it can be shown that there are initial conditions under which the energy at first goes from $(2k, 2\omega)$ wave to the (k, ω) wave, but even in that case eventually the entire energy is transferred to the $(2k, 2\omega)$ wave. This can be shown rigorously through Lyapunov stability theorem. Basically, the objective is to prove that $\mathcal{A}_1 = 0$ and $\mathcal{B}_2$ reaching its maximum is the asymptotically stable solution of the dynamical system described by equation (4.2).

To prove this, we first note that (4.2) can be put in the following form

$$\frac{\mathrm{d}}{\mathrm{d}x}\left(\mathcal{B}_2^2 - \frac{\alpha}{\beta}\mathcal{A}_1^2\right) = 0. \tag{4.12}$$

Therefore, since α/β can be shown to be always negative (see appendix B), we have

$$\mathcal{B}_2^2 - \frac{\alpha}{\beta}\mathcal{A}_1^2 = \mathcal{G}^2, \tag{4.13}$$

where $\mathcal{G}$ is a constant that is determined by the initial conditions. Equation (4.13) shows that $(\mathcal{A}_1, \mathcal{B}_2)$ are always moving on an ellipse. If we define a Lyapunov function $V(\mathcal{A}_1) = \mathcal{G} - \alpha/|\alpha|[\int_0^x \alpha\mathcal{A}_1(x)^2\,\mathrm{d}x + \mathcal{B}_2(0)]$, we find that $V(\mathcal{A}_1) \geqslant 0$ and $\mathrm{d}V/\mathrm{d}x < 0$. According to Lyapunov asymptotic stability theorem, the solution of the system converges to $\mathcal{A}_1 = 0$ from any starting points as x goes to ∞.

5. Conclusion

Here we reported that certain internal gravity waves are inherently unstable and are not able to sustain their form. This new instability mechanism, a result of resonant harmonic generation, draws the energy of an internal wave and hands it over to its second (or generally higher) harmonic. This resonance is distinguished from the classical triad resonance (and associated subharmonic instability) in that (i) a single wave may undergo the instability without requiring any external perturbation and (ii) the transfer of energy is irreversible and the original wave permanently loses its energy to its second harmonic. Extension of the results presented here to the third and higher harmonic generation is straightforward, but the strength of energy exchange in higher harmonics is much weaker.

Acknowledgements

We would like to thank Professor O. B. Fringer for the help with SUNTANS, and Dr J. Tchoufag and Dr L.-A. Couston for the careful reading of the manuscript and valuable comments. This publication was made possible, in part, with the support from NSF (grant no. CBET-1414579-EAGER) and the American Bureau of Shipping.

https://doi.org/10.1017/jfm.2016.754 Published online by Cambridge University Press

Appendix A. Derivation of the interaction equation

Consider the propagation of waves in an inviscid, incompressible, adiabatic and stably stratified fluid of density $\rho(x, y, z, t)$, bounded by a free surface on the top and a rigid sea floor with a depth h at the bottom. We consider a Cartesian coordinate system with x, y-axes on the mean free surface and z-axis positive upward. Equations governing the evolution of the velocity vector $\boldsymbol{u} = \{u, v, w\}$, density ρ, pressure p and surface elevation η under Boussinesq approximation read

$$\rho_0 \frac{\mathrm{D}\boldsymbol{u}}{\mathrm{D}t} = -\boldsymbol{\nabla} p - \rho g \boldsymbol{\nabla} z, \quad -h < z < \eta, \tag{A 1a}$$

$$\frac{\mathrm{D}\rho}{\mathrm{D}t} = 0, \quad -h < z < \eta, \tag{A 1b}$$

$$\boldsymbol{\nabla} \cdot \boldsymbol{u} = 0, \quad -h < z < \eta, \tag{A 1c}$$

$$\eta_t = \boldsymbol{u} \cdot \boldsymbol{\nabla}(z - \eta), \quad z = \eta, \tag{A 1d}$$

$$\frac{\mathrm{D}p}{\mathrm{D}t} = 0, \quad z = \eta, \tag{A 1e}$$

$$w = 0, \quad z = -h, \tag{A 1f}$$

where g is the gravitational acceleration and $\rho_0 = \bar{\rho}(z = 0)$ is the mean density on the free surface with $\bar{\rho}(z)$ the background (unperturbed) density such that $\rho = \bar{\rho}(z) + \rho'(x, y, z, t)$. Equation (A 1*a*) is the momentum equation, (A 1*b*) comes from conservation of salt in the absence of diffusion, mixing, sources and sinks, and (A 1*c*) is continuity equation that together form five equations for five unknown variables of the problem (three components of velocity $\boldsymbol{u}$, pressure p and density ρ). Equations (A 1*d*)–(A 1*f*) are boundary conditions on the free surface and the bottom.

Similar to the density perturbation ρ', we define a pressure perturbation p' via $p = \bar{p}(z) + p'(x, y, z, t)$ such that $\mathrm{d}\bar{p}(z)/\mathrm{d}z = -\bar{\rho}(z)g$. For the linear terms of the governing equation (A 1*a*) to be only in terms of w we calculate $\partial/\partial z[\boldsymbol{\nabla} \cdot (\text{A } 1a)] - \nabla^2(\text{A } 1a)_3$, where $(\text{A } 1a)_3$ denotes the z component of (A 1*a*) (likewise, 1,2 for x, y will be used later). We obtain

$$\frac{\partial}{\partial t}\nabla^2 w - \frac{\partial^2}{\partial x \partial z}\boldsymbol{u} \cdot \boldsymbol{\nabla} u - \frac{\partial^2}{\partial y \partial z}\boldsymbol{u} \cdot \boldsymbol{\nabla} v + \nabla_H^2(\boldsymbol{u} \cdot \boldsymbol{\nabla} w) + \frac{g}{\rho_0}\nabla_H^2 \rho' = 0, \tag{A 2}$$

where $\nabla_H^2 = \partial^2/\partial x^2 + \partial^2/\partial y^2$ is the horizontal Laplacian. Taking the time derivative of (A 2) and substituting ρ' from the expansion of (A 1*b*), i.e.

$$\frac{\partial \rho'}{\partial t} + \boldsymbol{u} \cdot \boldsymbol{\nabla} \rho' + w \frac{\mathrm{d}\bar{\rho}(z)}{\mathrm{d}z} = 0, \tag{A 3}$$

and denoting $N^2 = -(g/\rho_0)\,\mathrm{d}\bar{\rho}(z)/\mathrm{d}z$ as the Brunt–Väisälä frequency, we obtain

$$\begin{aligned}\frac{\partial^2}{\partial t^2}\nabla^2 w + N^2 \nabla_H^2 w \;=\; & \frac{\partial^3}{\partial x \partial z \partial t}\boldsymbol{u} \cdot \boldsymbol{\nabla} u + \frac{\partial^3}{\partial y \partial z \partial t}\boldsymbol{u} \cdot \boldsymbol{\nabla} v - \nabla_H^2 \frac{\partial}{\partial t}(\boldsymbol{u} \cdot \boldsymbol{\nabla} w) \\ & + \frac{g}{\rho_0}\nabla_H^2(\boldsymbol{u} \cdot \boldsymbol{\nabla} \rho').\end{aligned} \tag{A 4}$$

Expanding the surface dynamic boundary condition (A 1*e*) and keeping terms up to the second order we obtain

$$\frac{\partial p'}{\partial t} = w \rho_0 g - \boldsymbol{u} \cdot \boldsymbol{\nabla} p' - \frac{\partial^2 p'}{\partial z \partial t}\eta + \rho_0 g \eta \frac{\partial w}{\partial z} + g \eta w \frac{\mathrm{d}\bar{\rho}}{\mathrm{d}z}, \quad \text{at } z = 0, \tag{A 5}$$

https://doi.org/10.1017/jfm.2016.754 Published online by Cambridge University Press

where the last term can be equivalently written as $-N^2\bar{\rho}_0\eta w$. Since N^2 is much smaller than g in geophysical flows, this term will be dropped hereafter. Here p' can be substituted from an expression obtained from taking the x derivative of (A 1a)$_1$ added to the y derivative of (A 1a)$_2$ and taking the time derivative:

$$-\frac{\partial^3 w}{\partial z\partial t^2}+\frac{1}{\rho_0}\nabla_H^2\frac{\partial p'}{\partial t}+\frac{\partial^2}{\partial x\partial t}\boldsymbol{u}\cdot\boldsymbol{\nabla}u+\frac{\partial^2}{\partial y\partial t}\boldsymbol{u}\cdot\boldsymbol{\nabla}v=0. \tag{A 6}$$

Substituting $\partial p'/\partial t$ from (A 6) in (A 5) we obtain

$$\begin{aligned}\frac{\partial^3 w}{\partial z\partial t^2}-g\nabla_H^2 w \;=\;& \frac{\partial^2}{\partial x\partial t}\boldsymbol{u}\cdot\boldsymbol{\nabla}u+\frac{\partial^2}{\partial y\partial t}\boldsymbol{u}\cdot\boldsymbol{\nabla}v\\ &+\nabla_H^2\left(g\frac{\mathrm{d}w}{\mathrm{d}z}\eta\right)-\frac{1}{\rho_0}\nabla_H^2\left(\boldsymbol{u}\cdot\boldsymbol{\nabla}p'+\frac{\partial^2 p'}{\partial z\partial t}\eta\right).\end{aligned} \tag{A 7}$$

Therefore the governing equation and boundary conditions correct to $O(\epsilon^2)$ where ϵ is a measure of the wave steepness, reduce to (A 4), (A 7) and (A 1f). For the ease of reference, we rewrite these equations here:

$$\begin{aligned}\frac{\partial^2}{\partial t^2}\nabla^2 w+N^2\nabla_H^2 w \;=\;& \frac{\partial^3}{\partial x\partial z\partial t}\boldsymbol{u}\cdot\boldsymbol{\nabla}u+\frac{\partial^3}{\partial y\partial z\partial t}\boldsymbol{u}\cdot\boldsymbol{\nabla}v-\frac{\partial^3}{\partial x^2\partial t}\boldsymbol{u}\cdot\boldsymbol{\nabla}w\\ &-\frac{\partial^3}{\partial y^2\partial t}\boldsymbol{u}\cdot\boldsymbol{\nabla}w+\frac{g}{\rho_0}\nabla_H^2(\boldsymbol{u}\cdot\boldsymbol{\nabla}\rho') \quad -h<z<0,\end{aligned} \tag{A 8a}$$

$$\begin{aligned}\frac{\partial^3 w}{\partial z\partial t^2}-g\nabla_H^2 w \;=\;& \frac{\partial^2}{\partial x\partial t}\boldsymbol{u}\cdot\boldsymbol{\nabla}u+\frac{\partial^2}{\partial y\partial t}\boldsymbol{u}\cdot\boldsymbol{\nabla}v+\nabla_H^2\left(g\frac{\mathrm{d}w}{\mathrm{d}z}\eta\right)\\ &-\frac{1}{\rho_0}\nabla_H^2\left(\boldsymbol{u}\cdot\boldsymbol{\nabla}p'+\frac{\partial^2 p'}{\partial z\partial t}\eta\right) \quad z=0,\end{aligned} \tag{A 8b}$$

$$w=0, \quad z=-h. \tag{A 8c}$$

Equations (A 8a) and (A 8b) are equivalent to equations (A 2) and (A 7) of Thorpe (1966). (Except that we found three typos there: (i) for $S1$ in (A 2), the sign of the last term with g should be positive; (ii) for $S3$ in (A 7), the first term should be $\boldsymbol{\omega}\cdot\boldsymbol{\nabla}w$; and (iii) the term $g\nabla_1^2(\partial/\partial x)(\eta w_z)$ is missing. These are clearly typos as they do not appear in later expressions of Thorpe (1966).)

To perform a weakly nonlinear analysis, we assume that internal waves in the system described above are small perturbations from the mean state of water at rest, i.e. $\boldsymbol{u}$, ρ', $p'\sim O(\epsilon)$. Considering the two-dimensional problem and assuming that the solution to this problem can be expressed in terms of a convergent series we define

$$w(x,x_1,z,t)=\epsilon w_1(x,x_1,z,t)+\epsilon^2 w_2(x,x_1,z,t)+O(\epsilon^3), \tag{A 9}$$

where $x_1=\epsilon x$ is the slow spatial variable and $\epsilon\ll 1$ is a measure of steepness of the waves and $w_i\sim O(1)$. Similar expressions exist for other variables, i.e. $u=\epsilon u_1+\epsilon^2 u_2+O(\epsilon^3)$, $\rho'=\epsilon\rho_1'+\epsilon^2\rho_2'+O(\epsilon^3)$, $p'=\epsilon p_1'+\epsilon^2 p_2'+O(\epsilon^3)$ and $\eta=\epsilon\eta_1+\epsilon^2\eta_2+O(\epsilon^3)$ with u_i, ρ_i', $p_i'\sim O(1)$ being functions of x, x_1, z, t, and $\eta_i\sim O(1)$ being functions of x, x_1 and t.

Upon substitution into the governing equation, at the leading order $O(\epsilon)$ we obtain

$$\frac{\partial^2}{\partial t^2}\nabla^2 w_1+N^2\nabla_H^2 w_1=0, \quad -h<z<0, \tag{A 10a}$$

https://doi.org/10.1017/jfm.2016.754 Published online by Cambridge University Press

$$\frac{\partial^3 w_1}{\partial z \partial t^2} - g\nabla_H^2 w_1 = 0, \quad z = 0, \tag{A 10b}$$

$$w_1 = 0, \quad z = -h. \tag{A 10c}$$

At the second order $O(\epsilon^2)$ we have

$$\begin{aligned}\frac{\partial^2}{\partial t^2}\nabla^2 w_2 + N^2\nabla_H^2 w_2 \;=\; & -2\left(\frac{\partial^2}{\partial t^2} + N^2\right)\frac{\partial^2}{\partial x \partial x_1} w_1 + \frac{\partial^3}{\partial x \partial z \partial t}\boldsymbol{u}_1 \cdot \boldsymbol{\nabla} u_1 \\ & + \frac{\partial^3}{\partial y \partial z \partial t}\boldsymbol{u}_1 \cdot \boldsymbol{\nabla} v_1 - \frac{\partial^3}{\partial x^2 \partial t}\boldsymbol{u}_1 \cdot \boldsymbol{\nabla} w_1 - \frac{\partial^3}{\partial y^2 \partial t}\boldsymbol{u}_1 \cdot \boldsymbol{\nabla} w_1 \\ & + \frac{g}{\rho_0}\nabla_H^2(\boldsymbol{u}_1 \cdot \boldsymbol{\nabla}\rho_1'), \quad -h \leqslant z \leqslant 0. \end{aligned} \tag{A 11a}$$

$$\begin{aligned}\frac{\partial^3 w_2}{\partial z \partial t^2} - g\nabla_H^2 w_2 \;=\; & 2g\frac{\partial^2 w_1}{\partial x \partial x 1} + \frac{\partial^2}{\partial x \partial t}\boldsymbol{u}_1 \cdot \boldsymbol{\nabla} u_1 + \frac{\partial^2}{\partial y \partial t}\boldsymbol{u}_1 \cdot \boldsymbol{\nabla} v_1 \\ & + \nabla_H^2\left(g\frac{\mathrm{d}w_1}{\mathrm{d}z}\eta_1\right) \\ & - \frac{1}{\rho_0}\nabla_H^2\left(\boldsymbol{u}_1 \cdot \boldsymbol{\nabla} p_1' + \frac{\partial^2 p_1'}{\partial z \partial t}\eta_1\right), \quad z = 0, \end{aligned} \tag{A 11b}$$

$$w_2 = 0, \quad z = -h. \tag{A 11c}$$

We now assume that waves with wavenumber and frequency (k, ω) and $(2k, 2\omega)$ satisfy the internal waves dispersion relation (which is obtained from the linear equation (A 10))

$$\mathcal{D}(k, \omega) = \omega^2 - \frac{gk}{\sqrt{ga/\omega^2 - 1}} \tan\left(kh\sqrt{ga/\omega^2 - 1}\right), \tag{A 12}$$

i.e. $\mathcal{D}(k, \omega) = 0$ and $\mathcal{D}(2k, 2\omega) = 0$, and that they both exist in our domain of interest, though potentially with different amplitudes. The propagating wave solution to the linear equation (A 10) then obtains as

$$\begin{aligned} w_1(x, x_1, z, t) \;=\; & A_1(x_1)\sin m_1(z+h)\sin(kx - \omega t) + B_1(x_1)\sin m_1(z+h)\cos(kx - \omega t) \\ & + A_2(x_1)\sin m_2(z+h)\sin(2kx - 2\omega t) \\ & + B_2(x_1)\sin m_2(z+h)\cos(2kx - 2\omega t) \end{aligned} \tag{A 13}$$

in which A_1, A_2, B_1, B_2 are amplitudes of each wave, $m_1^2 = k^2(N^2 - \omega^2)/\omega^2$ and $m_2^2 = k^2(N^2 - 4\omega^2)/\omega^2$. Other variables u, ρ', p' and η can be found respectively via continuity equation (A 1*c*), equation for conservation of salt (A 1*b*), kinematic surface boundary condition (A 1*d*) and the dynamic free surface boundary condition (A 1*f*).

The left-hand side of the second-order equation (A 11) is identical in the form to the first-order equation (A 10), but the right-hand side of (A 11) is clearly non-zero and is a nonlinear function of the leading-order solution $\boldsymbol{u}_1$, ρ_1', p_1', η_1. It turns out, after substitution, that the right-hand side contains terms with harmonics which are the same as the harmonics of the leading-order equation (secular terms). A compatibility condition then must be enforced to make sure that the solution does not go unbounded, which is clearly unphysical. This compatibility condition determines the spatial behaviour of the coefficients A_i, B_i.

https://doi.org/10.1017/jfm.2016.754 Published online by Cambridge University Press

While the formulation presented here is general, our primary interest is when an initial wave with wavenumber and frequency (k, ω) resonates with its second harmonic $(2k, 2\omega)$ whose initial amplitude is zero. Therefore in the following we use the adjectives original and resonant waves to refer to (k, ω) and $(2k, 2\omega)$ waves respectively. We would like to emphasize that the formulation is general and works for any initial condition of the two waves. We will also comment that the presented approach can be easily extended to third- and higher-harmonic generation.

Without loss of generality we assume that $B_1 = 0$, which only has to do with our choice of coordinate system. But we keep A_2 and B_2, since they determine the phase of the resonant wave $(2k, 2\omega)$ with respect to the original wave (k, ω). The general solution to the second-order problem takes the form

$$w_2(x, x_1, z, t) = C_{11}(x_1, z)\sin(kx - \omega t) + C_{12}(x_1, z)\cos(kx - \omega t) \quad (A\,14a)$$
$$+ C_{21}(x_1, z)\sin(2kx - 2\omega t) + C_{22}(x_1, z)\cos(2kx - 2\omega t), \quad (A\,14b)$$

where the values of $C_{ij}(x_1, z)$ are to be determined from (A 11). Substituting (A 14) and (A 13) into (A 11), and collecting same sine and cosine terms we obtain four ordinary differential equations for C_{ij} $(i, j = 1, 2)$:

$$-\omega^2 C_{1i,zz} - m_1^2\omega^2 C_{1i} = E_{1i}, \quad -h < z < 0, \quad (A\,15a)$$
$$-\omega^2 C_{1i,z} + gk^2 C_{1i} = F_{1i}, \quad z = 0, \quad (A\,15b)$$
$$C_{1i} = 0, \quad z = -h, \quad (A\,15c)$$
$$-4\omega^2 C_{2i,zz} - 4m_2^2\omega^2 C_{2i} = E_{2i}, \quad -h < z < 0, \quad (A\,16a)$$
$$-4\omega^2 C_{2i,z} + 4gk^2 C_{2i} = F_{2i}, \quad z = 0, \quad (A\,16b)$$
$$C_{2i} = 0, \quad z = -h, \quad (A\,16c)$$

where E_{i1}, F_{i1} are the coefficients of $\sin(ikx - i\omega t)$, and E_{i2}, F_{i2} are the coefficients of $\cos(ikx - i\omega t)$ in the right-hand side of (A 11*a*) and (A 11*b*) respectively. Let us first consider the equation for C_{22}, we obtain

$$E_{22} = -\frac{4\omega^2 m_2^2}{k}\sin m_2(z + h)\frac{\mathrm{d}A_2(x_1)}{\mathrm{d}x_1}, \quad F_{22} = 4gk\sin m_2 h\frac{\mathrm{d}A_2(x_1)}{\mathrm{d}x_1}, \quad (A\,17a,b)$$

for which the solution to (A 16*a*) that satisfies the boundary condition (A 16*c*) is

$$C_{22}(x_1, z) = -\frac{m_2}{2k}(z + h)\cos m_2(z + h)\frac{\mathrm{d}A_2(x_1)}{\mathrm{d}x_1}. \quad (A\,18)$$

Upon substitution into (A 16*b*) we obtain

$$gk\left(\frac{2m_2 h + \sin 2m_2 h}{\cos m_2 h}\right)\frac{\mathrm{d}A_2(x_1)}{\mathrm{d}x_1} = 0, \quad (A\,19)$$

therefore, since the coefficient is non-zero then $\mathrm{d}A_2/\mathrm{d}x_1 \equiv 0$. Physically speaking, this expression says that the amplitude A_2 does not change as waves propagate, or in other words, A_2 does not take part in the energy exchange. We, therefore, set A_2 equal to zero for the rest of the derivation. Physically, this means that the second harmonic must have a $\pi/2$ radian phase difference relative to the original wave.

https://doi.org/10.1017/jfm.2016.754 Published online by Cambridge University Press

We use the same approach as above for C_{21}. We have

$$E_{21} = \frac{4\omega^2 m_2^2}{k} \sin m_2(z+h) \frac{\mathrm{d}B_2(x_1)}{\mathrm{d}x_1}, \tag{A 20a}$$

$$F_{21} = -4gk \sin m_2 h \frac{\mathrm{d}B_2}{\mathrm{d}x_1} - 6\omega m_1^2 A_1^2(x_1), \tag{A 20b}$$

for which

$$C_{21}(x_1, z) = \frac{m_2}{2k}(z+h) \cos m_2(z+h) \frac{\mathrm{d}B_2(x_1)}{\mathrm{d}x_1}, \tag{A 21}$$

and upon substitution into (A 16*b*) we obtain

$$\frac{\mathrm{d}B_2(x_1)}{\mathrm{d}x_1} = \alpha A_1^2(x_1), \tag{A 22}$$

where

$$\alpha = -\frac{6m_1^2 \omega \cos m_2 h}{gk(2m_2 h + \sin 2m_2 h)}. \tag{A 23}$$

For $C_{11}(x_1, z)$, we obtain $E_{11} = F_{11} = 0$ and therefore the equation for $C_{11}(x_1, z)$ does not provide any extra information on $A_1(x_1)$ and $B_2(x_1)$. For C_{12} we obtain

$$\begin{aligned} E_{12} \;=\; & \frac{2m_1^2\omega^2}{k} \sin m_1(z+h) \frac{\mathrm{d}A_1(x_1)}{\mathrm{d}x_1} \\ & + \{I^+ \sin[(m_1+m_2)(z+h)] + I^- \sin[(m_1-m_2)(z+h)]\} A_1(x_1) B_2(x_1), \end{aligned} \tag{A 24}$$

$$F_{12} = 2gk \sin m_1(z+h) \frac{\mathrm{d}A_1(x_1)}{\mathrm{d}x_1} + JA_1(x_1)B_2(x_1), \tag{A 25}$$

where

$$I^+ = \tfrac{1}{8}\omega(m_2 + 2m_1)(m_2^2 + 3k^2 - m_1^2), \tag{A 26a}$$

$$I^- = \tfrac{1}{8}\omega(2m_1 - m_2)(m_1^2 - 3k^2 - m_2^2), \tag{A 26b}$$

$$J = \frac{1}{4} \frac{gk^2(4m_1 \cos^2 m_1 h \sin m_2 h - 2m_2 \cos m_2 h \sin 2m_1 h - 3m_1 \sin m_2 h)}{\omega \cos m_1 h}. \tag{A 26c}$$

We obtain

$$\begin{aligned} C_{12}(x_1, z) \;=\; & -\frac{m_1}{k}(z+h) \cos m_1(z+h) \frac{\mathrm{d}A_1(x_1)}{\mathrm{d}x_1} \\ & + \left\{ \frac{I^+ \sin[(m_1+m_2)(z+h)]}{\omega^2[m_1^2 - (m_1+m_2)^2]} + \frac{I^- \sin[(m_1-m_2)(z+h)]}{\omega^2[m_1^2 - (m_1-m_2)^2]} \right\} A_1(x_1) B_2(x_1). \end{aligned} \tag{A 27}$$

Substituting into (A 15*b*), we obtain

$$\frac{\mathrm{d}A_1(x_1)}{\mathrm{d}x_1} = \beta A_1(x_1) B_2(x_1), \tag{A 28}$$

https://doi.org/10.1017/jfm.2016.754 Published online by Cambridge University Press

where

$$\beta = -\frac{k[\sin m_2h(4m_1\cos^2 m_1h - 3m_1) - 2m_2\cos m_2h\sin 2m_1h]}{2\omega(2m_1h + \sin 2m_1h)}. \tag{A 29}$$

If we define the actual amplitudes $\mathcal{A}_1 = \epsilon A_1$ and $\mathcal{B}_2 = \epsilon B_2$ (note that $w = \epsilon w_1 + O(\epsilon^2)$) then

$$\frac{\mathrm{d}\mathcal{B}_2}{\mathrm{d}x} = \alpha\mathcal{A}_1^2, \tag{A 30a}$$

$$\frac{\mathrm{d}\mathcal{A}_1}{\mathrm{d}x} = \beta\mathcal{A}_1\mathcal{B}_2, \tag{A 30b}$$

with the same α, β repeated here:

$$\alpha = -\frac{6m_1^2\omega\cos m_2h}{gk(2m_2h + \sin 2m_2h)}, \tag{A 31a}$$

$$\beta = -\frac{k[\sin m_2h(4m_1\cos^2 m_1h - 3m_1) - 2m_2\cos m_2h\sin 2m_1h]}{2\omega(2m_1h + \sin 2m_1h)}. \tag{A 31b}$$

Appendix B. Proof of the sign of α/β

For the sign of α/β, we have

$$\mathrm{sign}\left(\frac{\alpha}{\beta}\right) = \mathrm{sign}\left[\frac{\cos m_2h}{\sin m_2h(4m_1\cos^2 m_1h - 3m_1) - 2m_2\cos m_2h\sin 2m_1h}\right]. \tag{B 1}$$

It is equivalent to the sign of

$$\tan m_2h(4m_1\cos^2 m_1h - 3m_1) - 2m_2\sin 2m_1h. \tag{B 2}$$

Rearranging terms of the above expression gives,

$$\cos^2 m_1h(4m_1\tan m_2h - 4m_2\tan m_1h) - 3m_1\tan m_2h. \tag{B 3}$$

After substitution of the dispersion relation,

$$\omega^2 = \frac{gk^2}{m_1}\tan m_1h \tag{B 4}$$

and

$$\omega^2 = \frac{gk^2}{m_2}\tan m_2h. \tag{B 5}$$

Equation (B 3) can be simplified to

$$-3m_1\tan m_2h = -3m_1m_2\frac{\omega^2}{gk^2}, \tag{B 6}$$

which is always less than zero.

REFERENCES

ALAM, M.-R. 2012 A new triad resonance between co-propagating surface and interfacial waves. *J. Fluid Mech.* **691**, 267–278.

ALAM, M.-R., LIU, Y. & YUE, D. K. P. 2009*a* Bragg resonance of waves in a two-layer fluid propagating over bottom ripples. Part 1. Perturbation analysis. *J. Fluid Mech.* **624**, 191–224.

https://doi.org/10.1017/jfm.2016.754 Published online by Cambridge University Press

ALAM, M.-R., LIU, Y. & YUE, D. K. P. 2009*b* Bragg resonance of waves in a two-layer fluid propagating over bottom ripples. Part 2. Numerical simulation. *J. Fluid Mech.* **624**, 225–253.

ALAM, M.-R., LIU, Y. & YUE, D. K. P. 2010 Oblique sub-and super-harmonic Bragg resonance of surface waves by bottom ripples. *J. Fluid Mech.* **643**, 437–447.

ALAM, M.-R., LIU, Y. & YUE, D. K. P. 2011 Resonant-wave signature of an oscillating and translating disturbance in a two-layer density stratified fluid. *J. Fluid Mech.* **675**, 477–494.

ALAM, M.-R. & MEI, C. C. 2007 Attenuation of long interfacial waves over a randomly rough seabed. *J. Fluid Mech.* **587**, 73–96.

ALFORD, M. H., PEACOCK, T., MACKINNON, J. A., NASH, J. D., BUIJSMAN, M. C., CENTURONI, L. R., CHAO, S.-Y., CHANG, M.-H., FARMER, D. M., FRINGER, O. B. *et al.* 2015 The formation and fate of internal waves in the south china sea. *Nature* **521** (7550), 65–69.

BOYD, P. W. 2007 Biogeochemistry: iron findings. *Nature* **446** (7139), 989–991.

BÜHLER, O. & HOLMES-CERFON, M. 2011 Decay of an internal tide due to random topography in the ocean. *J. Fluid Mech.* **678**, 271–293.

COUSTON, L.-A., LIANG, Y. & ALAM, M.-R. 2016 Oblique chain resonance of internal waves by three-dimensional seabed corrugations. Preprint, arXiv:1604.07308.

DAVIS, R. E. & ACRIVOS, A. 1967 The stability of oscillatory internal waves. *J. Fluid Mech.* **30** (04), 723–736.

FERRARI, R. & WUNSCH, C. 2008 Ocean circulation kinetic energy: reservoirs, sources, and sinks. *Annu. Rev. Fluid Mech.* **41** (1), 253–282.

FRINGER, O. B., GERRITSEN, M. & STREET, R. L. 2006 An unstructured-grid, finite-volume, nonhydrostatic, parallel coastal ocean simulator. *Ocean Model.* **14** (3–4), 139–173.

GARRETT, C. 2003 Oceanography: mixing with latitude. *Nature* **422** (6931), 477.

GERKEMA, T., STAQUET, C. & BOURUET-AUBERTOT, P. 2006 Decay of semi-diurnal internal-tide beams due to subharmonic resonance. *Geophys. Res. Lett.* **33** (8), L08604.

HARRIS, G. P. 1986 *Phytoplankton Ecology: Structure, Function and Fluctuation*. Chapman and Hall.

HASSELMANN, K. 1967 A criterion for nonlinear wave stability. *J. Fluid Mech.* **30** (04), 737–739.

JIANG, C.-H. & MARCUS, P. S. 2009 Selection rules for the nonlinear interaction of internal gravity waves. *Phys. Rev. Lett.* **102** (12), 124502.

KANG, D. & FRINGER, O. 2010 On the calculation of available potential energy in internal wave fields. *J. Phys. Oceanogr.* **40** (11), 2539–2545.

KANG, D. & FRINGER, O. 2012 Energetics of barotropic and baroclinic tides in the monterey bay area. *J. Phys. Oceanogr.* **42** (2), 272–290.

KARIMPOUR, F., ZAREEI, A. & ALAM, M.-R. 2016 Sensitivity of internal wave energy distribution over seabed corrugations to adjacent seabed features. Preprint, arXiv:1604.02641.

MACKINNON, J. A. & WINTERS, K. B. 2005 Subtropical catastrophe: significant loss of low-mode tidal energy at 28.9. *Geophys. Res. Lett.* **32** (15), L15605.

MARTIN, S., SIMMONS, W. & WUNSCH, C. 1972 The excitation of resonant triads by single internal waves. *J. Fluid Mech.* **53**, 17–44.

MCCOMAS, C. H. & BRETHERTON, F. P. 1977 Resonant interaction of oceanic internal waves. *J. Geophys. Res.* **82** (9), 1397–1412.

MCEWAN, A. D. 1971 Degeneration of resonantly-excited standing internal gravity waves. *J. Fluid Mech.* **50** (03), 431–448.

MULLER, P. 1986 Nonlinear interactions among internal gravity waves. *Rev. Geophys.* **24** (3), 493–536.

SCOLAN, H., ERMANYUK, E. & DAUXOIS, T. 2013 Nonlinear fate of internal wave attractors. *Phys. Rev. Lett.* **110** (23), 234501.

STAQUET, C. & SOMMERIA, J. 2002 Internal gravity waves: from instabilities to turbulence. *Annu. Rev. Fluid Mech.* **34**, 559–593.

SUTHERLAND, B. R. 2016 Excitation of superharmonics by internal modes in non-uniformly stratified fluid. *J. Fluid Mech.* **793**, 335–352.

TABAEI, A., AKYLAS, T. R. & LAMB, K. G. 2005 Nonlinear effects in reflecting and colliding internal wave beams. *J. Fluid Mech.* **526**, 217–243.

THORPE, S. A. 1966 On wave interactions in a stratified fluid. *J. Fluid Mech.* **24**, 737–751.

https://doi.org/10.1017/jfm.2016.754 Published online by Cambridge University Press

THORPE, S. A. 1968 On the shape of progressive internal waves. *Phil. Trans. R. Soc. Lond.* A **263** (1145), 563–614.

WALTER, R. K., WOODSON, C. B., ARTHUR, R. S., FRINGER, O. B. & MONISMITH, S. G. 2012 Nearshore internal bores and turbulent mixing in southern monterey bay. *J. Geophys. Res.* **117** (C07017), 1–13.

WANG, B., GIDDINGS, S. N., FRINGER, O. B., GROSS, E. S., FONG, D. A. & MONISMITH, S. G. 2011 Modeling and understanding turbulent mixing in a macrotidal salt wedge estuary. *J. Geophys. Res.* **116** (C02036), 1–23.

WUNSCH, S. 2015 Nonlinear harmonic generation by diurnal tides. *Dyn. Atmos. Oceans* **71**, 91–97.

ZHANG, H. P., KING, B. & SWINNEY, H. L. 2008 Resonant generation of internal waves on a model continental slope. *Phys. Rev. Lett.* **100** (24), 244504.

ZHANG, Z., FRINGER, O. B. & RAMP, S. R. 2011 Three-dimensional, nonhydrostatic numerical simulation of nonlinear internal wave generation and propagation in the South China Sea. *J. Geophys. Res.* **116**, C05022 1–26.

https://doi.org/10.1017/jfm.2016.754 Published online by Cambridge University Press